Critical line of $2 + 1$ flavor QCD: Toward the continuum limit

Paolo Cea[*]

Dipartimento di Fisica dell'Università di Bari and INFN—Sezione di Bari, I-70126 Bari, Italy

Leonardo Cosmai[†]

INFN—Sezione di Bari, I-70126 Bari, Italy

Alessandro Papa[‡]

Dipartimento di Fisica dell'Università della Calabria and INFN—Gruppo collegato di Cosenza, I-87036 Arcavacata di Rende, Cosenza, Italy

We determine the continuum limit of the curvature of the pseudocritical line of QCD with $n_f = 2 + 1$ staggered fermions at nonzero temperature and quark density. We perform Monte Carlo simulations at imaginary baryon chemical potentials with Highly Improved Staggered Quarks (HISQ), adopting the HISQ/tree action discretization as implemented in the code by the MILC Collaboration. Couplings are adjusted so as to move on a line of constant physics, as determined in Ref. [1], with the strange quark mass m_s fixed at its physical value and a light-to-strange mass ratio $m_l/m_s = 1/20$. The chemical potential is set at the same value for the three quark species, $\mu_l = \mu_s \equiv \mu$. We attempt an extrapolation to the continuum using the results on lattices with temporal size up to $L_t = 12$. Our estimate for the continuum value of the curvature κ at zero baryon density, $\kappa = 0.020(4)$, is compared with recent lattice results and with experimental determinations of the freeze-out curve.

I. INTRODUCTION

The phase diagram of strongly interacting matter in the temperature (T)-baryon density plane remains a challenge for theoretical physics. Although there is little doubt that it features a low-temperature hadronic phase, with broken chiral symmetry, and a high-temperature deconfined phase, with restored chiral symmetry, the question about the precise location and the exact nature of the transition between these two phases is still open. Yet, the answer to this question has many phenomenological implications: the region of the phase diagram with high T and small baryon density is relevant for the physics of the early Universe, whereas the region of low T and high baryon density is interesting for the astrophysics of some compact objects, but other corners of the phase diagram are not less interesting (see Ref. [2] for an overview).

Relativistic heavy-ion collisions provide us with a unique opportunity to infer properties of the transition: depending on the energy of the ion beams and on the mass number of the colliding ions, the fireball generated in the collision could fulfill the temperature and baryon density conditions under which the deconfined phase appears as a transient state, before the system freezes out into hadrons, which are then detected. Thermal-statistical models, assuming approximate chemical equilibrium at the chemical

freeze-out point, are able to describe the particle yields at a given collision energy in terms of two parameters only, the freeze-out temperature T and the baryon chemical potential μ_B. The collection of freeze-out parameters extracted from experiments with different collision energy lie on a curve in the (T, μ_B) plane, extending up to $\mu_B \lesssim 800$ MeV (see Fig. 1 of Ref. [3], or Ref. [4] for a recent reanalysis of experimental data).

QCD is widely accepted as the theory of strong interactions and, as such, must encode all the information needed to precisely draw the phase diagram in the (T, μ_B) plane. As a matter of fact, only some corners of it can be accessed by first-principle applications of QCD, in the perturbative or in the nonperturbative regime. Here, we focus on the lattice approach of QCD, based on the idea of discretizing the theory on a Euclidean space-time lattice and simulating it by Monte Carlo numerical simulations as a statistical system, with Boltzmann weight given by $\exp(-S_E)$, where S_E is the QCD Euclidean action. The region of the phase diagram where $\mu_B/(3T) \lesssim 1$ is within the reach of this approach, and one can therefore address, at least inside this region, the problem of determining the shape taken by the QCD pseudocritical line separating the hadronic from the deconfined phase.

There is no *a priori* argument for the coincidence of the QCD pseudocritical line with the chemical freeze-out curve: if the deconfined phase is realized in the fireball, in cooling down, the system first rehadronizes, then reaches the chemical freeze-out. This implies that the freeze-out

[*]paolo.cea@ba.infn.it
[†]leonardo.cosmai@ba.infn.it
[‡]papa@cs.infn.it

curve lies below the pseudocritical line in the $\mu_B - T$ plane. It is a common working hypothesis that the delay between chemical freeze-out and rehadronization is so short that the two curves lie close to each other and can therefore be compared. Under the assumptions of charge-conjugation invariance at $\mu_B = 0$ and analyticity around this point, the QCD pseudocritical line, as well as the freeze-out curve, can be parametrized, at low baryon densities, by a lowest-order expansion in the dimensionless quantity $\mu_B/T(\mu_B)$, as

$$\frac{T(\mu_B)}{T_c(0)} = 1 - \kappa \left(\frac{\mu_B}{T(\mu_B)} \right)^2 + \ldots, \qquad (1)$$

where $T_c(0)$ and κ are, respectively, the pseudocritical temperature and the curvature at vanishing baryon density.

Direct Monte Carlo simulations of lattice QCD at non-zero baryon density are hindered by the well-known "sign problem": S_E becomes complex, and the Boltzmann weight loses its sense. Several ways out of this problem have been devised (see Ref. [5] for a review): redesigning the Monte Carlo updating algorithms for a complex action [6], reweighting from the ensemble at $\mu_B = 0$ [7], Taylor expanding the relevant observables around $\mu_B = 0$ and calculating the first coefficients of the series by simulations at $\mu_B = 0$ [8–10], using the canonical formulation [11,12], using the density of states method [13], and simulating the theory at imaginary chemical potentials and performing the analytic continuation to real ones [14–21].

The numerical evidence gathered so far in QCD with $n_f = 2 + 1$ and physical or almost physical quark masses points to a scenario with a smooth crossover between the hadronic and the deconfined (or chirally symmetric) phase at $\mu_B = 0$, with a pseudocritical temperature $T_c(0)$ of about 155 MeV [1,22]. This crossover behavior should persist in some neighborhood of $\mu_B = 0$, up to the onset of a first-order transition at some value of $\mu_B > 0$.

The state of the art of lattice determinations of the curvature κ, up to the very recent papers of Refs. [20,21], is summarized in Fig. 10 of Ref. [19]: depending on the lattice setup and on the observable used to probe the transition, the value of κ can change even by almost a factor of 3. The lattice setup dependence stems from the kind of adopted discretization, the lattice size, the choice of quark masses and chemical potentials, and the procedure to circumvent the sign problem. This dependence would totally disappear if, ideally, all groups would use the same lattice setup. A contribution to the understanding of the impact of the lattice setup dependence is provided in Appendix B of Ref. [19]. The dependence on the probe observable is, instead, irreducible: since a smooth crossover is taking place rather than a true phase transition, one cannot define a *bona fide* order parameter of which the behavior would permit uniquely locating the transition point; instead, for any adopted surrogate observable, a different transition point should be expected, at least in principle.

On the side of the determinations of the freeze-out curve, two recent determinations [3,4] of κ, both based on the thermal-statistical model, but the latter of them including the effect of inelastic collisions after freeze-out, give two quite different values of κ, each seeming to prefer a different subset of lattice results (see Fig. 3 of Ref. [18] for a snapshot of the situation).

The aim of this work is to contribute to a better understanding of the systematics underlying lattice determinations of the curvature κ, by corroborating our previous determination [18] with an extrapolation to the continuum limit and by comparing it with experimental analyses of the freeze-out curve.

Our lattice setup is as follows. We simulate the HISQ/tree action of the MILC Collaboration with $2 + 1$ staggered fermions on lattices with the temporal extension $L_t = 6, 8, 10,$ and 12 and aspect ratio equal to 4. We work on the line of constant physics as determined in Ref. [1], with the strange mass set at the physical value and the light quark mass fixed at $m_l = m_s/20$. As discussed in Ref. [1], this amounts to tuning the strange quark mass until the mass of the fictitious $\eta_{s\bar{s}}$ meson matches the lowest-order perturbation theory estimate $m_{\eta_{s\bar{s}}} = \sqrt{2m_K^2 - m_\pi^2}$. Consequently, within our simulations, the pion mass is $m_\pi \simeq 160$ MeV.

We perform simulations at imaginary quark chemical potentials, assigning the same value to the three quark species, $\mu_l = \mu_s \equiv \mu$, then extrapolate to real chemical potentials. Our probe observables are the disconnected susceptibility of the light quark chiral condensate and its renormalized counterpart. Simulating the theory at imaginary chemical potentials poses no restriction on the lattice size or in the choice of the couplings. However, the periodicity in $\text{Im}(\mu_l)/T$ of the partition function [23] implies that the information gathered outside a narrow interval of imaginary chemical potentials is redundant. For the setup with $\mu_l = \mu_s \equiv \mu$, this interval can be chosen as the region $0 \leq \text{Im}(\mu)/T \leq \pi/3$. A safe extrapolation of the critical line to real chemical potentials requires that it exhibits a smooth dependence on imaginary chemical potential over this interval, a condition which must be checked to be satisfied *a posteriori* by our data.

The preference to the disconnected susceptibility of the light quark chiral condensate has multiple motivations [1]. First of all, for small enough quark masses, its contribution to the chiral susceptibility dominates over the connected one, which is harder to compute; then, it shows a strong sensitivity to the transition; finally, it is exempt from additive renormalization, undergoing only a multiplicative one. This translates into a very precise determination of the critical couplings at imaginary μ, which is the main prerequisite of a safe extrapolation to the real values of μ.

There are two main limitations in our setup. The first is that we work with a physical strange quark mass, but with light quarks a bit heavier than physical ones. Numerical results in $n_f = 2$ indicate a mild dependence of the

curvature on the quark mass (see the discussion in Sec. III of Ref. [17]). If the same applies here, as we believe, our result for κ will only slightly underestimate (in an absolute value) the true physical curvature. The second limitation is that, for the sake of comparison with the freeze-out curve, our setup of chemical potentials could not be the one which better reproduces the initial conditions of heavy ion collision. In fact, strangeness neutrality would rather impose $\mu_s \lesssim \mu_l$. In general, the setup $\mu_l = \mu_s = \mu_B/3$ approximates strangeness neutrality at low temperatures, while the $\mu_s = 0$ setup is relevant for high enough temperatures. It is natural to expect that the effect of taking $\mu_s = \mu_l$ instead of $\mu_s = 0$ becomes less and less evident when μ_l/T approaches zero, so that the curvature κ at zero baryon density should not differ too much in the two cases. The numerical analysis of Refs. [19–21] has shown that this effect is invisible within the accuracy of the lattice setup adopted there.

The paper is organized as follows. In Sec. II, we give some further details of our numerical simulations. In Sec. III, we show our numerical results for κ. Finally, in Sec. IV, we draw our conclusions.

II. SIMULATION DETAILS AND NUMERICAL RESULTS

We perform simulations of lattice QCD with $2 + 1$ flavors of rooted staggered quarks at imaginary quark chemical potential. We have made use of the HISQ/tree action [24–26] as implemented in the publicly available MILC code [27], which has been suitably modified by us in order to introduce an imaginary quark chemical potential $\mu = \mu_B/3$. That has been done by multiplying all forward and backward temporal links entering the discretized Dirac operator by $\exp(ia\mu)$ and $\exp(-ia\mu)$, respectively; in this way, the fermion determinant is still real and positive so that standard Monte Carlo methods can be applied. As already remarked above, in the present study, we have $\mu = \mu_l = \mu_s$. This means that the Euclidean partition function of the discretized theory reads

$$Z = \int [DU] e^{-S_{\text{gauge}}} \prod_{q=u,d,s} \det(D_q[U,\mu])^{1/4}, \quad (2)$$

where S_{gauge} is the Symanzik-improved gauge action and $D_q[U,\mu]$ is the staggered Dirac operator, modified as explained above for the inclusion of the imaginary quark chemical (see Ref. [25] and Appendix A of Ref. [26] for the precise definition of the gauge action and the covariant derivative for highly improved staggered fermions).

All simulations make use of the rational hybrid Monte Carlo (RHMC) algorithm. The length of each RHMC trajectory has been set to 1.0 in molecular dynamics time units.

We have simulated the theory at finite temperature, and for several values of the imaginary quark chemical potential, near the transition temperature, adopting lattices of size $16^3 \times 6$, $24^3 \times 6$, $32^3 \times 8$, $40^3 \times 10$, and $48^3 \times 12$. We have discarded typically not less than 1000 trajectories for each run and have collected from 4000 to 8000 trajectories for measurements.

The pseudocritical point $\beta_c(\mu^2)$ has been determined as the value for which the renormalized disconnected susceptibility of the light quark chiral condensate divided by T^2 exhibits a peak. The bare disconnected susceptibility is given by

$$\chi_{1,\text{disc}} = \frac{n_f^2}{16 L_s^3 L_t} \{ \langle (\text{Tr}D_q^{-1})^2 \rangle - \langle \text{Tr}D_q^{-1} \rangle^2 \}. \quad (3)$$

Here, $n_f = 2$ is the number of light flavors, and L_s denotes the lattice size in the space direction. The renormalized chiral susceptibility is defined as

$$\chi_{1,\text{ren}} = \frac{1}{Z_m^2} \chi_{1,\text{disc}}. \quad (4)$$

The multiplicative renormalization factor Z_m can be deduced from an analysis of the line of constant physics for the light quark masses. More precisely, we have [26]

$$Z_m(\beta) = \frac{m_l(\beta)}{m_l(\beta^*)}, \quad (5)$$

where the renormalization point β^* is chosen such that

$$\frac{r_1}{a(\beta^*)} = 2.37, \quad (6)$$

where the function $a(\beta)$ is discussed below. In Fig. 1 is shown the multiplicative renormalization factor Z_m determined in the case when r_1 is used to set the scale (see below). To precisely localize the peak in $\chi_{1,\text{ren}}/T^2$, a Lorentzian fit has been used. For illustrative purposes, in Fig. 2, we display our determination of the pseudocritical couplings at $\mu/(\pi T) = 0.2i$ for all lattices considered in this work. The complete collection of results for the disconnected susceptibility of the light quark chiral condensate obtained in this work is presented in the Appendix.

To get the ratios $T_c(\mu)/T_c(0)$, we fix the lattice spacing through the observables r_1 and f_K, following the discussion in Appendix B of Ref. [1]. For the r_1 scale, the lattice spacing is given in terms of the r_1 parameter as
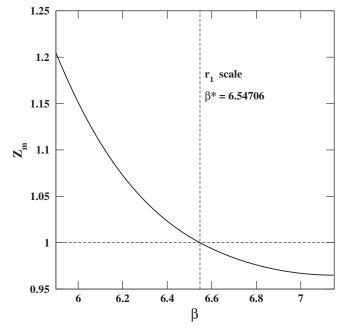
FIG. 1.   The multiplicative renormalization factor Z_m in the case of the r_1 scale. The renormalization point is $\beta^* = 6.54706$.

$$\frac{a}{r_1}(\beta)_{m_l=0.05m_s} = \frac{c_0 f(\beta) + c_2 (10/\beta) f^3(\beta)}{1 + d_2 (10/\beta) f^2(\beta)}, \quad (7)$$

with $c_0 = 44.06$, $c_2 = 272102$, $d_2 = 4281$, and $r_1 = 0.3106(20)$ fm. On the other hand, in the case of the f_K scale, we have

$$a f_K(\beta)_{m_l=0.05m_s} = \frac{c_0^K f(\beta) + c_2^K (10/\beta) f^3(\beta)}{1 + d_2^K (10/\beta) f^2(\beta)}, \quad (8)$$

with $c_0^K = 7.66$, $c_2^K = 32911$, $d_2^K = 2388$, and $r_1 f_K \simeq 0.1738$. In Eqs. (7) and (8), $f(\beta)$ is the two-loop beta function,

$$f(\beta) = (b_0 (10/\beta))^{-b_1/(2b_0^2)} \exp(-\beta/(20 b_0)), \quad (9)$$

b_0 and b_1 being its universal coefficients.

Our results are summarized in Table I. For all lattice sizes but $24^3 \times 6$ (where we have only one value of μ), the behavior of $T_c(\mu)/T_c(0)$ can be nicely fitted with a linear function in μ^2,

$$\frac{T_c(\mu)}{T_c(0)} = 1 + R_q \left(\frac{i\mu}{\pi T_c(\mu)} \right)^2, \quad (10)$$

which gives us access to the curvature R_q and, hence, to the curvature parameter $\kappa = -R_q/(9\pi^2)$ introduced in Eq. (1). On the $24^3 \times 6$ lattice, the linearity in μ^2 has been assumed to hold, in order to extract R_q from the only available determination at $\mu/(\pi T) = 0.2i$.

For the sake of the extrapolation to the continuum limit, in Fig. 3, we report our determinations of R_q on the lattices $24^3 \times 6$, $32^3 \times 8$, $40^3 \times 10$, and $48^3 \times 12$ and from the two different methods to set the scale, vs $1/L_t^2$.

Within our accuracy, cutoff effects on R_q are negligible so that a constant fit works well over the whole region
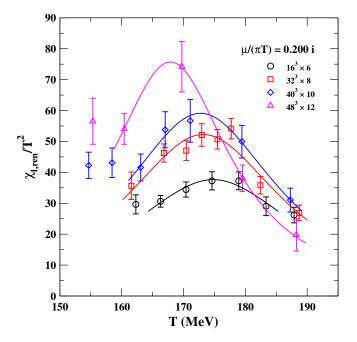

FIG. 2.   The real part of the renormalized susceptibility of the light quark chiral condensate over T^2 on the lattices $16^3 \times 6$, $32^3 \times 8$, $40^3 \times 10$, and $48^3 \times 12$ at $\mu/(\pi T) = 0.2i$. Full lines give the Lorentzian fits near the peaks. The temperature has been determined from the r_1 scale.

TABLE I.   Summary of the values of the ratio $T_c(\mu)/T_c(0)$ for the imaginary quark chemical potentials μ considered in this work. The data for $\mu = 0$ on the $24^3 \times 6$, $32^3 \times 68$, and $48^3 \times 12$ lattices have been estimated from the disconnected chiral susceptibilities reported, respectively, in Tables X, XI, and XII of Ref. [1]. The datum for $\mu = 0$ on the $40^3 \times 10$ lattice has been estimated from the disconnected chiral susceptibilities reported in Table XI of Ref. [28]. The values of $T_c(\mu)/T_c(0)$ evaluated fixing the lattice scale by r_1 and f_K are reported, respectively, in the third and in the fourth columns of the table.

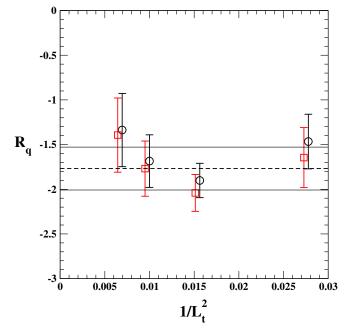| Lattice	$\mu/(\pi T)$	$T_c(\mu)/T_c(0)$ (r_1 scale)	$T_c(\mu)/T_c(0)$ (f_K scale)
$16^3 \times 6$	$0.15i$	1.038(13)	1.043(14)
	$0.2i$	1.063(15)	1.070(15)
	$0.25i$	1.085(16)	1.095(18)
$24^3 \times 6$	$0.2i$	1.061(9)	1.067(10)
$32^3 \times 8$	$0.15i$	1.054(7)	1.059(8)
	$0.2i$	1.066(10)	1.071(11)
	$0.25i$	1.117(10)	1.126(10)
$40^3 \times 10$	$0.15i$	1.023(23)	1.024(24)
	$0.2i$	1.075(14)	1.079(15)
	$0.25i$	1.102(15)	1.107(15)
$48^3 \times 12$	$0.15i$	1.013(31)	1.013(33)
	$0.20i$	1.051(14)	1.052(15)
	$0.25i$	1.094(26)	1.097(25)

FIG. 3. Determinations of the curvature R_q on the lattices $24^3 \times 6$, $32^3 \times 8$, $40^3 \times 10$, and $48^3 \times 12$ and from the two different methods to set the scale, vs $1/L_t^2$. Data points related with the f_K scale setting have been slightly shifted along the horizontal axis for better readability. The dashed horizontal line gives the result of the fit to all data with a constant; the solid horizontal lines indicate the uncertainty on this constant (95% confidence level).

($\chi_r^2 \simeq 0.99$), thus including also the smallest $24^3 \times 6$ lattice. Taking into account the uncertainties due to the continuum limit extrapolation,

$$\kappa = 0.020(4). \tag{11}$$

Our estimate of the uncertainties for the curvature given in Eq. (11) takes into account both the error in the fit minimization and the choice of the minimization function. We stress, however, that if we exclude from the fit the value on the lattice with the smallest L_t, i.e., the rightmost points in Fig. 3, the extrapolation to the continuum becomes largely undetermined. Indeed, with the values of R_q obtained in the present work (see Table II), the fit with a constant is rather stable even if $L_t = 6$ is excluded, but the fit with a linear function in $1/L_t^2$ in the latter case gives a much smaller value of the curvature κ, though with a large uncertainty (see Table III).

TABLE III. Summary of the fit of the curvature κ with the function $\kappa(L_t) = \kappa + A/L_t^2$, with A taken equal to zero or left free. The first column specifies the values of L_t included in the fit, and the last column specifies the reduced χ^2. The uncertainties on the fit parameters are obtained with 70% confidence level.

L_t included	κ	A	χ_r^2
6, 8, 10, 12	0.01991(114)	0.	0.76
6, 8, 10, 12	0.02014(449)	−0.015(259)	0.89
8, 10, 12	0.02048(127)	0.	0.80
8, 10, 12	0.01182(748)	0.669(559)	0.14

III. CONCLUSIONS AND DISCUSSION

We have studied QCD with $n_f = 2 + 1$ flavors discretized in the HISQ/tree rooted staggered fermion formulation and in the presence of an imaginary baryon chemical potential, with a physical strange quark mass and a light-to-strange mass ratio $m_l/m_s = 1/20$, and $\mu = \mu_l = \mu_s$.

We have estimated, by the method of analytic continuation, the continuum limit of the curvature of the pseudocritical line in the temperature-baryon chemical potential, defined in Eq. (1). The observable adopted to identify, for each fixed μ, the crossover temperature has been the disconnected part of the renormalized susceptibility of the light quark chiral condensate, in units of the squared temperature. This observable is convenient for many reasons: it dominates, for small enough quark masses, the whole light chiral susceptibility, which would be much harder to implement; it undergoes only a multiplicative renormalization; it is strongly sensitive to the transition, thus allowing precise determinations of the pseudocritical temperatures.

We have found that, within the accuracy of our determinations, cutoff effects on the curvature are negligible already on the lattice with temporal size $L_t = 6$. Our determination of the curvature parameter, $\kappa = 0.020(4)$, is indeed compatible with the value quoted in our previous paper [18], $\kappa = 0.018(4)$, without the extrapolation to the continuum.

It is interesting to extrapolate the critical line as determined in this work to the region of real baryon density and compare it with the freeze-out curves resulting from a few phenomenological analyses of relativistic heavy-ion collisions. This is done in Fig. 4, where we report two different estimates. The first is from the analysis of Ref. [3], based on

TABLE II. Summary of determinations of the curvature R_q for all values of L_t considered in this work and from the two different methods to set the scale.

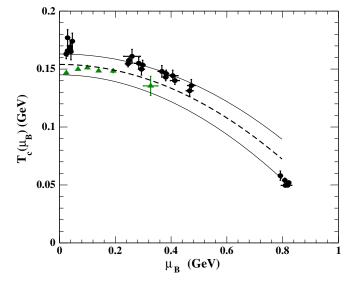| L_t	6	8	10	12
R_q (r_1 scale)	−1.466(306)	−1.902(192)	−1.685(294)	−1.337(410)
κ (r_1 scale)	0.017(3)	0.021(2)	0.019(3)	0.015(5)
R_q (f_K scale)	−1.646(336)	−2.041(206)	−1.769(309)	−1.394(415)
κ (r_K scale)	0.019(4)	0.023(2)	0.020(3)	0.016(5)

FIG. 4. $T_c(\mu_B)$ vs μ_B (units in GeV). Experimental values of $T_c(\mu_B)$ are taken from Fig. 1 of Ref. [3] (black circles) and from Fig. 3 of Ref. [29] (green triangles), for the standard hadronization model and for the susceptibilities of conserved charges, respectively. The dashed line is a parametrization corresponding to $T_c(\mu_B) = T_c(0) - b\mu_B^2$ with $T_c(0) = 0.154(9)$ GeV and $b = 0.128(25)$ GeV^{-1}. The solid lines represent the corresponding error band.

the standard statistical hadronization model, where the freeze-out curve is parametrized as

$$T_c(\mu_B) = a - b\mu_B^2 - c\mu_B^4, \qquad (12)$$

with $a = 0.166(2)$ GeV, $b = 0.139(16)$ GeV^{-1}, and $c = 0.053(21)$ GeV^{-3}. The second estimate is from Ref. [29] and is based on the analysis of susceptibilities of the (conserved) baryon and electric charges. In fact, our critical line is in nice agreement with all the freeze-out points of Refs. [3,29]. In particular, using our estimate of the curvature, Eq. (11), we get $b = 0.128(25)$ GeV^{-1}, in very good agreement with the quoted phenomenological value. The significance of the comparison presented in Fig. 4, with special reference to the question whether the pseudocritical line lies indeed above the freeze-out curve, can be increased at the (non-negligible) price of reducing the uncertainties on $T_c(0)$ and on κ.

Some *caveats* are in order here. We do not expect our critical line to be reliable too far from $\mu = 0$; as a rule of thumb, we can trust it up to real quark chemical potentials of the same order of the modulus of the largest imaginary chemical potential included in the fit (10), i.e., $|\mu|/(\pi T) = 0.25$. This translates to real baryon chemical potentials in the region $\mu_B \lesssim 0.4$ GeV. Moreover, the effect of taking $\mu_s = \mu_l$ instead of $\mu_s < \mu_l$ should become visible on the shape of the critical line as we move away from $\mu = 0$ in the region of real baryon densities, thus reducing

further the region of reliability of our critical line. So, from a prudential point of view, the agreement shown in Fig. 4 could be considered the fortunate combination of different kinds of systematic effects. We cannot, however, exclude the possibility that the message from Fig. 4 is to be interpreted in positive sense; i.e., the setup we adopted and the observable we considered may catch better some features of the crossover transition, thus explaining the nice comparison with freeze-out data. Indeed, our result for the continuum extrapolation of the curvature κ is in fair agreement with the recent estimates in Ref. [20], where both setup $\mu_s = \mu_l$ and $\mu_s = 0$ were adopted, and Ref. [21], where the strangeness neutral trajectories were determined from lattice simulations by imposing $\langle n_S \rangle = 0$.

APPENDIX: SUMMARY OF DATA FOR THE DISCONNECTED SUSCEPTIBILITY OF THE LIGHT QUARK CHIRAL CONDENSATE

In this Appendix (Tables IV–XVI), we summarize all the results for the disconnected chiral susceptibility obtained in our simulations for each considered value of the coupling β and for the corresponding physical temperature, as determined from the two different procedures to set the scale.

TABLE IV. Data for the disconnected chiral susceptibility on the $16^3 \times 6$ lattice at $\mu/(\pi T) = 0.150i$: the second column gives $\chi_{l,\mathrm{disc}}$ defined in Eq. (3), and the fourth and sixth columns give $\chi_{l,\mathrm{ren}}/T^2$, with $\chi_{l,\mathrm{ren}}$ defined in Eq. (4) and the temperature T (columns three and five, respectively) determined by the two different methods to set the scale.

β	$\chi_{l,\mathrm{disc}}$	T(MeV) (r_1 scale)	$\chi_{l,\mathrm{ren}}/T^2$	T(MeV) (f_K scale)	$\chi_{l,\mathrm{ren}}/T^2$
6.000	0.939 (0.114)	147.3	25.5 (3.1)	138.2	27.7 (3.4)
6.050	0.495 (0.134)	154.6	14.0 (3.8)	145.8	15.0 (4.1)
6.100	1.133 (0.145)	162.3	33.2 (4.3)	153.8	35.4 (4.5)
6.125	1.260 (0.089)	166.3	37.6 (2.6)	158.0	39.8 (2.8)
6.150	1.273 (0.079)	170.4	38.6 (2.4)	162.3	40.7 (2.5)
6.175	1.187 (0.086)	174.6	36.6 (2.7)	166.7	38.4 (2.8)
6.195	1.093 (0.107)	178.1	34.1 (3.3)	170.2	35.6 (3.5)
6.200	0.944 (0.100)	178.9	29.5 (3.1)	171.1	30.8 (3.3)

TABLE V. Data for the disconnected chiral susceptibility on the $16^3 \times 6$ lattice at $\mu/(\pi T) = 0.200i$ (legend as in Table IV).

β	$\chi_{l,\mathrm{disc}}$	$T(\mathrm{MeV})$ (r_1 scale)	$\chi_{l,\mathrm{ren}}/T^2$	$T(\mathrm{MeV})$ (f_K scale)	$\chi_{l,\mathrm{ren}}/T^2$
6.100	1.010 (0.105)	162.3	29.6 (3.1)	153.8	31.5 (3.3)
6.125	1.026 (0.063)	166.3	30.6 (1.9)	158.0	32.4 (2.0)
6.150	1.135 (0.081)	170.4	34.4 (2.5)	162.3	36.3 (2.6)
6.175	1.208 (0.095)	174.6	37.2 (2.9)	166.7	39.1 (3.1)
6.200	1.191 (0.093)	178.9	37.3 (2.9)	171.1	38.9 (3.0)
6.225	0.915 (0.095)	183.4	29.0 (3.0)	175.8	30.2 (3.2)
6.250	0.814 (0.078)	187.9	26.2 (2.5)	180.5	27.1 (2.6)

TABLE VI. Data for the disconnected chiral susceptibility on the $16^3 \times 6$ lattice at $\mu/(\pi T) = 0.250i$ (legend as in Table IV).

β	$\chi_{l,\mathrm{disc}}$	$T(\mathrm{MeV})$ (r_1 scale)	$\chi_{l,\mathrm{ren}}/T^2$	$T(\mathrm{MeV})$ (f_K scale)	$\chi_{l,\mathrm{ren}}/T^2$
6.150	0.899 (0.095)	170.4	27.3 (2.9)	162.3	28.8 (3.0)
6.180	1.089 (0.064)	175.5	33.7 (2.0)	167.5	35.3 (2.1)
6.186	1.078 (0.083)	176.5	33.5 (2.6)	168.6	35.0 (2.7)
6.200	1.117 (0.097)	178.9	34.9 (3.0)	171.1	36.5 (3.2)
6.250	0.784 (0.066)	187.9	25.2 (2.1)	180.5	26.1 (2.2)
6.300	0.561 (0.051)	197.3	18.5 (1.7)	190.2	19.0 (1.7)
6.350	0.189 (0.047)	207.2	6.4 (1.6)	200.5	6.5 (1.6)

TABLE VII. Data for the disconnected chiral susceptibility on the $24^3 \times 6$ lattice at $\mu/(\pi T) = 0.200i$ (legend as in Table IV).

β	$\chi_{l,\mathrm{disc}}$	$T(\mathrm{MeV})$ (r_1 scale)	$\chi_{l,\mathrm{ren}}/T^2$	$T(\mathrm{MeV})$ (f_K scale)	$\chi_{l,\mathrm{ren}}/T^2$
6.120	0.916 (0.107)	165.5	27.3 (3.2)	157.2	28.9 (3.4)
6.150	1.106 (0.136)	170.4	33.6 (4.1)	162.3	35.4 (4.4)
6.165	0.849 (0.079)	172.9	26.0 (2.4)	164.9	27.3 (2.5)
6.180	1.084 (0.073)	175.5	33.5 (2.3)	167.5	35.1 (2.4)
6.195	1.288 (0.078)	178.1	40.2 (2.4)	170.2	42.0 (2.5)
6.210	1.159 (0.087)	180.7	36.5 (2.7)	173.0	38.0 (2.9)
6.225	1.244 (0.098)	183.4	39.5 (3.1)	175.8	41.1 (3.2)
6.240	1.030 (0.070)	186.1	33.0 (2.2)	178.6	34.2 (2.3)
6.255	0.979 (0.160)	188.8	31.6 (5.1)	181.4	32.7 (5.3)
6.270	0.692 (0.062)	191.6	22.5 (2.0)	184.3	23.2 (2.1)
6.300	0.430 (0.038)	197.3	14.2 (1.2)	190.2	14.6 (1.3)

TABLE VIII. Data for the disconnected chiral susceptibility on the $32^3 \times 8$ lattice at $\mu/(\pi T) = 0.150i$ (legend as in Table IV).

β	$\chi_{l,\mathrm{disc}}$	$T(\mathrm{MeV})$ (r_1 scale)	$\chi_{l,\mathrm{ren}}/T^2$	$T(\mathrm{MeV})$ (f_K scale)	$\chi_{l,\mathrm{ren}}/T^2$
6.415	0.646 (0.073)	165.5	39.7 (4.5)	160.9	40.1 (4.6)
6.424	0.730 (0.047)	167.0	45.0 (2.9)	162.4	45.5 (3.0)
6.429	0.780 (0.035)	167.8	48.2 (2.2)	163.2	48.6 (2.2)
6.436	0.865 (0.059)	169.0	53.6 (3.7)	164.4	54.1 (3.7)
6.450	0.962 (0.047)	171.3	59.8 (3.0)	166.8	60.3 (3.0)
6.460	0.883 (0.070)	173.0	55.1 (4.4)	168.6	55.4 (4.4)
6.470	0.776 (0.060)	174.6	48.6 (3.8)	170.3	48.8 (3.8)

TABLE IX. Data for the disconnected chiral susceptibility on the $32^3 \times 8$ lattice at $\mu/(\pi T) = 0.200i$ (legend as in Table IV).

β	$\chi_{l,\mathrm{disc}}$	$T(\mathrm{MeV})$ (r_1 scale)	$\chi_{l,\mathrm{ren}}/T^2$	$T(\mathrm{MeV})$ (f_K scale)	$\chi_{l,\mathrm{ren}}/T^2$
6.390	0.585 (0.073)	161.7	35.6 (4.4)	156.8	36.2 (4.5)
6.423	0.751 (0.048)	166.8	46.3 (3.0)	162.2	46.8 (3.0)
6.445	0.757 (0.051)	170.4	47.0 (3.2)	166.0	47.4 (3.2)
6.460	0.834 (0.058)	173.0	52.1 (3.6)	168.6	52.4 (3.7)
6.475	0.808 (0.051)	175.5	50.7 (3.2)	171.2	50.9 (3.2)
6.488	0.860 (0.053)	177.7	54.2 (3.3)	173.5	54.3 (3.3)
6.515	0.565 (0.045)	182.4	35.8 (2.8)	178.3	35.8 (2.8)
6.550	0.420 (0.039)	188.7	26.9 (2.5)	184.8	26.8 (2.5)

TABLE X. Data for the disconnected chiral susceptibility on the $32^3 \times 8$ lattice at $\mu/(\pi T) = 0.250i$ (legend as in Table IV).

β	$\chi_{l,\mathrm{disc}}$	$T(\mathrm{MeV})$ (r_1 scale)	$\chi_{l,\mathrm{ren}}/T^2$	$T(\mathrm{MeV})$ (f_K scale)	$\chi_{l,\mathrm{ren}}/T^2$
6.420	0.613 (0.055)	166.4	37.7 (3.4)	161.7	38.2 (3.4)
6.455	0.555 (0.044)	172.1	34.6 (2.7)	167.7	34.8 (2.7)
6.490	0.792 (0.053)	178.1	49.9 (3.4)	173.8	50.0 (3.4)
6.525	0.753 (0.051)	184.2	47.8 (3.3)	180.2	47.8 (3.3)
6.560	0.568 (0.030)	190.6	36.5 (2.0)	186.7	36.3 (1.9)

TABLE XI. Data for the disconnected chiral susceptibility on the $40^3 \times 10$ lattice at $\mu/(\pi T) = 0.150i$ (legend as in Table IV).

β	$\chi_{l,\mathrm{disc}}$	$T(\mathrm{MeV})$ (r_1 scale)	$\chi_{l,\mathrm{ren}}/T^2$	$T(\mathrm{MeV})$ (f_K scale)	$\chi_{l,\mathrm{ren}}/T^2$
6.550	0.444 (0.043)	151.0	44.4 (4.3)	147.9	44.3 (4.3)
6.606	0.570 (0.070)	159.4	57.9 (7.1)	156.5	57.4 (7.0)
6.648	0.524 (0.037)	165.9	53.6 (3.8)	163.2	53.0 (3.8)
6.690	0.525 (0.048)	172.7	54.1 (4.9)	170.2	53.3 (4.8)
6.732	0.402 (0.035)	179.8	41.7 (3.6)	177.4	41.0 (3.5)

TABLE XII. Data for the disconnected chiral susceptibility on the $40^3 \times 10$ lattice at $\mu/(\pi T) = 0.200i$ (legend as in Table IV).

β	$\chi_{l,\mathrm{disc}}$	$T(\mathrm{MeV})$ (r_1 scale)	$\chi_{l,\mathrm{ren}}/T^2$	$T(\mathrm{MeV})$ (f_K scale)	$\chi_{l,\mathrm{ren}}/T^2$
6.575	0.420 (0.042)	154.7	42.3 (4.3)	151.7	42.0 (4.2)
6.600	0.425 (0.047)	158.4	43.1 (4.8)	155.5	42.7 (4.7)
6.630	0.407 (0.043)	163.1	41.6 (4.4)	160.3	41.1 (4.3)
6.655	0.525 (0.057)	167.0	53.8 (5.8)	164.4	53.1 (5.8)
6.680	0.550 (0.067)	171.1	56.7 (6.9)	168.5	55.8 (6.8)
6.730	0.481 (0.051)	179.4	49.9 (5.3)	177.1	49.0 (5.2)
6.775	0.297 (0.037)	187.3	31.0 (3.9)	185.1	30.4 (3.8)

TABLE XIII. Data for the disconnected chiral susceptibility on the $40^3 \times 10$ lattice at $\mu/(\pi T) = 0.250i$ (legend as in Table IV).

β	$\chi_{l,\mathrm{disc}}$	$T(\mathrm{MeV})$ (r_1 scale)	$\chi_{l,\mathrm{ren}}/T^2$	$T(\mathrm{MeV})$ (f_K scale)	$\chi_{l,\mathrm{ren}}/T^2$
6.645	0.386 (0.060)	165.4	39.5 (6.1)	162.7	39.0 (6.1)
6.664	0.368 (0.041)	168.5	37.8 (4.2)	165.8	37.3 (4.1)
6.714	0.552 (0.064)	176.7	57.2 (6.6)	174.3	56.3 (6.5)
6.764	0.421 (0.059)	185.3	43.9 (6.1)	183.1	43.0 (6.0)
6.810	0.193 (0.051)	193.6	20.2 (5.3)	191.5	19.8 (5.2)

TABLE XV. Data for the disconnected chiral susceptibility on the $48^3 \times 12$ lattice at $\mu/(\pi T) = 0.200i$ (legend as in Table XVI).

β	$\chi_{l,\mathrm{disc}}$	$T(\mathrm{MeV})$ (r_1 scale)	$\chi_{l,\mathrm{ren}}/T^2$	$T(\mathrm{MeV})$ (f_K scale)	$\chi_{l,\mathrm{ren}}/T^2$
6.770	0.376 (0.049)	155.3	56.5 (7.4)	153.5	55.3 (7.3)
6.804	0.357 (0.033)	160.4	54.0 (5.0)	158.6	52.8 (4.8)
6.864	0.487 (0.054)	169.7	74.2 (8.2)	168.1	72.2 (8.0)
6.924	0.249 (0.028)	179.5	38.1 (4.3)	178.1	37.0 (4.2)
6.975	0.129 (0.034)	188.3	19.8 (5.2)	186.9	19.2 (5.1)

TABLE XIV. Data for the disconnected chiral susceptibility on the $48^3 \times 12$ lattice at $\mu/(\pi T) = 0.150i$ (legend as in Table IV).

β	$\chi_{l,\mathrm{disc}}$	$T(\mathrm{MeV})$ (r_1 scale)	$\chi_{l,\mathrm{ren}}/T^2$	$T(\mathrm{MeV})$ (f_K scale)	$\chi_{l,\mathrm{ren}}/T^2$
6.700	0.242 (0.052)	145.3	36.1 (7.7)	145.3	36.1 (7.7)
6.730	0.374 (0.047)	149.5	55.9 (7.1)	149.5	55.9 (7.1)
6.780	0.433 (0.063)	156.8	65.3 (9.5)	156.8	65.3 (9.5)
6.815	0.475 (0.111)	162.1	71.9 (16.8)	162.1	71.9 (16.8)
6.830	0.382 (0.036)	164.4	57.9 (5.5)	164.4	57.9 (5.5)
6.880	0.466 (0.068)	172.3	71.1 (10.4)	172.3	71.1 (10.4)
6.930	0.247 (0.027)	180.5	37.8 (4.1)	180.5	37.8 (4.1)
6.980	0.191 (0.032)	189.1	29.3 (4.9)	189.1	29.3 (4.9)

TABLE XVI. Data for the disconnected chiral susceptibility on the $48^3 \times 12$ lattice at $\mu/(\pi T) = 0.250i$ (legend as in Table IV).

β	$\chi_{l,\mathrm{disc}}$	$T(\mathrm{MeV})$ (r_1 scale)	$\chi_{l,\mathrm{ren}}/T^2$	$T(\mathrm{MeV})$ (f_K scale)	$\chi_{l,\mathrm{ren}}/T^2$
6.650	0.274 (0.044)	138.5	40.4 (6.5)	136.3	39.9 (6.4)
6.750	0.175 (0.054)	152.4	26.3 (8.1)	150.5	25.8 (8.0)
6.864	0.300 (0.042)	169.7	45.7 (6.3)	168.1	44.5 (6.2)
6.900	0.418 (0.043)	175.6	64.0 (6.6)	174.1	62.2 (6.4)
6.950	0.278 (0.037)	183.9	42.6 (5.6)	182.6	41.4 (5.4)
6.975	0.224 (0.025)	188.3	34.4 (3.8)	186.9	33.4 (3.7)
7.025	0.153 (0.018)	197.2	23.6 (2.7)	196.0	22.8 (2.6)

[1] A. Bazavov *et al.*, Phys. Rev. D **85**, 054503 (2012).
[2] M. Stephanov, *Proc. Sci.*, LATTICE2006 (2006) 024.
[3] J. Cleymans, H. Oeschler, K. Redlich, and S. Wheaton, Phys. Rev. C **73**, 034905 (2006).
[4] F. Becattini M. Bleicher, T. Kollegger, T. Schuster, J. Steinheimer, and R. Stock, Phys. Rev. Lett. **111**, 082302 (2013).
[5] O. Philipsen, *Proc. Sci.*, LATTICE2005 (2006) 016; C. Schmidt, *Proc. Sci.*, LATTICE2006 (2006) 021; P. de Forcrand, *Proc. Sci.*, LATTICE2009 (2009) 010; G. Aarts, *Proc. Sci.*, LATTICE2012 (2012) 017.
[6] F. Karsch and H. Wyld, Phys. Rev. Lett. **55**, 2242 (1985); G. Aarts, E. Seiler, and I.-O. Stamatescu, Phys. Rev. D **81**, 054508 (2010); G. Aarts, F. A. James, E. Seiler, and I.-O. Stamatescu, Eur. Phys. J. C **71**, 1756 (2011); G. Aarts and F. A. James, J. High Energy Phys. 01 (2012) 118; E. Seiler, D. Sexty, and I.-O. Stamatescu, Phys. Lett. B **723**, 213 (2013); G. Aarts, L. Bongiovanni, E. Seiler, D. Sexty, and I.-O. Stamatescu, Eur. Phys. J. A **49**, 89 (2013); D. Sexty, Phys. Lett. B **729**, 108 (2014).
[7] I. M. Barbour, S. E. Morrison, E. G. Klepfish, J. B. Kogut, and M.-P. Lombardo, Phys. Rev. D **56**, 7063 (1997); Z. Fodor and S. Katz, Phys. Lett. B **534**, 87 (2002); J. High Energy Phys. 03 (2002) 014; J. High Energy Phys. 04 (2004) 050.
[8] S. A. Gottlieb, W. Liu, D. Toussaint, R. Renken, and R. Sugar, Phys. Rev. D **38**, 2888 (1988); S. Choe *et al.*

(QCD-TARO Collaboration), Nucl. Phys. **A698**, 395 (2002); S. Choe *et al.*, Phys. Rev. D **65**, 054501 (2002); C. R. Allton, S. Ejiri, S. J. Hands, O. Kaczmarek, F. Karsch, E. Laermann, C. Schmidt, and L. Scorzato, Phys. Rev. D **66**, 074507 (2002).
[9] C. R. Allton, S. Ejiri, S. J. Hands, O. Kaczmarek, F. Karsch, E. Laermann, and C. Schmidt, Phys. Rev. D **68**, 014507 (2003); **71**, 054508 (2005); S. Ejiri, F. Karsch, E. Laermann, and C. Schmidt, Phys. Rev. D **73**, 054506 (2006).
[10] G. Endrodi, Z. Fodor, S. Katz, and K. Szabo, J. High Energy Phys. 04 (2011) 001; Sz. Borsányi, G. Endrődi, Z. Fodor, S. D. Katz, S. Krieg, C. Ratti, and K. K. Szabo, J. High Energy Phys. 08 (2012) 053.
[11] M. G. Alford, A. Kapustin, and F. Wilczek, Phys. Rev. D **59**, 054502 (1999); A. Hasenfratz and D. Toussaint, Nucl. Phys. **B371**, 539 (1992); S. Kratochvila and P. de Forcrand, *Proc. Sci.*, LATTICE2005 (2006) 167; A. Alexandru, M. Faber, I. Horvath, and K.-F. Liu, Phys. Rev. D **72**, 114513 (2005).
[12] P. de Forcrand and S. Kratochvila, Nucl. Phys. B, Proc. Suppl. **153**, 62 (2006).
[13] G. Bhanot, K. Bitar, and R. Salvador, Phys. Lett. B **188**, 246 (1987); M. Karliner, S. R. Sharpe, and Y. Chang, Nucl. Phys. **B302**, 204 (1988); V. Azcoiti, G. di Carlo, and A. Grillo, Phys. Rev. Lett. **65**, 2239 (1990); J. Ambjorn, K. Anagnostopoulos, J. Nishimura, and J. Verbaarschot, J. High Energy Phys. 10 (2002) 062.

[14] M.-P. Lombardo, Nucl. Phys. B, Proc. Suppl. **83–84,** 375 (2000); P. de Forcrand and O. Philipsen, Nucl. Phys. **B642,** 290 (2002); **B673,** 170 (2003); M. D'Elia and M.-P. Lombardo, Phys. Rev. D **67,** 014505 (2003); **70,** 074509 (2004); V. Azcoiti, G. Di Carlo, A. Galante, and V. Laliena, Nucl. Phys. **B723,** 77 (2005); P. de Forcrand and O. Philipsen, J. High Energy Phys. 01 (2007) 077; 11 (2008) 012; P. de Forcrand, S. Kim, and O. Philipsen, Proc. Sci., LATTICE2007 (2007)178.

[15] P. Cea, L. Cosmai, M. D'Elia, and A. Papa, Phys. Rev. D **81,** 094502 (2010).

[16] P. Cea, L. Cosmai, M. D'Elia, and A. Papa, Proc. Sci., LATTICE2010 (2010) 173; P. Cea, L. Cosmai, M. D'Elia, A. Papa, and F. Sanfilippo, Proc. Sci., LATTICE2012 (2012) 067.

[17] P. Cea, L. Cosmai, M. D'Elia, A. Papa, and F. Sanfilippo, Phys. Rev. D **85,** 094512 (2012); L.-K. Wu, X.-Q. Luo, and H.-S. Chen, Phys. Rev. D **76,** 034505 (2007); K. Nagata and A. Nakamura, Phys. Rev. D **83,** 114507 (2011); P. Giudice and A. Papa, Phys. Rev. D **69,** 094509 (2004); Nucl. Phys. B, Proc. Suppl. **140,** 529 (2005); A. Papa, P. Cea, L. Cosmai, and M. D'Elia, Proc. Sci., LATTICE2006 (2006) 143; P. Cea, L. Cosmai, M. D'Elia, and A. Papa, Proc. Sci., LATTICE2007 (2007) 214; Proc. Sci., LATTICE2009 (2009) 192; P. Cea, L. Cosmai, M. D'Elia, C. Manneschi, and A. Papa, Phys. Rev. D **80,** 034501 (2009); Proc. Sci., LATTICE2009 (2009) 161; F. Karbstein and M. Thies, Phys. Rev. D **75,** 025003 (2007).

[18] P. Cea, L. Cosmai, and A. Papa, Phys. Rev. D **89,** 074512 (2014).

[19] C. Bonati, M. D'Elia, M. Mariti, M. Mesiti, F. Negro, and F. Sanfilippo, Phys. Rev. D **90,** 114025 (2014).

[20] C. Bonati, M. D'Elia, M. Mariti, M. Mesiti, F. Negro, and F. Sanfilippo, Phys. Rev. D **92,** 054503 (2015).

[21] R. Bellwied, S. Borsanyi, Z. Fodor, J. Gnther, S. D. Katz, C. Ratti, and K. K. Szabo, Phys. Lett. B **751,** 559 (2015).

[22] Y. Aoki, Z. Fodor, S. Katz, and K. Szabo, Phys. Lett. B **643,** 46 (2006); Y. Aoki, G. Endrodi, Z. Fodor, S. Katz, and K. Szabo, Nature (London) **443,** 675 (2006); Y. Aoki S. Borsányi, S. Dürr, Z. Fodor, S. D Katz, S. Krieg, and K. Szabo et al., J. High Energy Phys. 06 (2009) 088; T. Bhattacharya et al., Phys. Rev. Lett. **113,** 082001 (2014).

[23] A. Roberge and N. Weiss, Nucl. Phys. **B275,** 734 (1986).

[24] E. Follana, Q. Mason C. Davies, K. Hornbostel, G. P. Lepage, J. Shigemitsu, H. Trottier, and K. Wong (HPQCD Collaboration, UKQCD Collaboration), Phys. Rev. D **75,** 054502 (2007).

[25] A. Bazavov (MILC Collaboration), Rev. Mod. Phys. **82,** 1349 (2010).

[26] A. Bazavov et al. (MILC Collaboration), Phys. Rev. D **82,** 074501 (2010).

[27] http://physics.utah.edu/~detar/milc/.

[28] A. Bazavov et al. (HotQCD Collaboration), Phys. Rev. D **90,** 094503 (2014).

[29] P. Alba, W. Alberico, R. Bellwied M. Bluhm, V. M. Sarti, M. Nahrgang, and C. Ratti, Phys. Lett. B **738,** 305 (2014).